energies

MDPI

Article

Comparison of Measured and Derived Thermal Conductivities in the Unsaturated Soil Zone of a Large-Scale Geothermal Collector System (LSC)

Mario Rammler *, Hans Schwarz, Jan Wagner and David Bertermann

GeoZentrum Nordbayern, Department Geographie und Geowissenschaften, Friedrich-Alexander-Universität Erlangen-Nürnberg, Schlossgarten 5, 91054 Erlangen, Germany
* Correspondence: mario.rammler@fau.de

Abstract: The design, energetic performance, and thermal impact of large-scale geothermal collector systems (LSCs) are dependent on the thermal conductivity of unsaturated soils (λ). The aim of this study was to investigate the benefits of two different λ measurement methods using single-needle sensor measuring devices on a laboratory scale. Since large-scale determinations are required in the context of LSCs, the potential for deriving λ from electrical resistivity tomography measurements (ERTs) was also examined. Using two approaches—the continuous evaporation method and the punctual method—thermal conductivities of soil samples from Bad Nauheim (Germany) were measured. The results were compared with averaged λ derived from three ERT sections. With the evaporation method, significant bulk density changes were observed during the experimental procedure, which were caused by the clay content and the use of repacked samples. The punctual method ensures a sufficiently constant bulk density during the measurements, but only provides a small number of measurement points. The thermal conductivities derived from ERTs show largely minor deviations from the laboratory measurements on average. If further research confirms the results of this study, ERTs could provide a non-invasive and unelaborate thermal exploration of the subsurface in the context of large-scale infrastructure projects such as LSCs.

Keywords: large-scale geothermal collector system (LSC); thermal conductivity of soils; single-needle sensor; electrical resistivity tomography (ERT); shrinkage of soils; unsaturated soil zone

Citation: Rammler, M.; Schwarz, H.; Wagner, J.; Bertermann, D. Comparison of Measured and Derived Thermal Conductivities in the Unsaturated Soil Zone of a Large-Scale Geothermal Collector System (LSC). *Energies* **2023**, *16*, 1195. https://doi.org/10.3390/en16031195

Academic Editors: Alessandro Casasso and Adriana Angelotti

Received: 23 December 2022
Revised: 17 January 2023
Accepted: 18 January 2023
Published: 21 January 2023

1. Introduction

1.1. Large-Scale Geothermal Collector System (LSC) in Bad Nauheim (Germany)

For reaching the aims of climate policies, reducing emissions not only from power production but also from heat supply is necessary [1]. Thereby, shallow geothermal energy is an important component of achieving these goals. In addition to standard systems, such as borehole heat exchangers or small-scale horizontal systems for individual residential or industrial buildings, the focus is also shifting to a combination of fifth-generation district heating and cooling networks with, for example, large-scale geothermal collector systems (LSCs) [2]. LSCs are defined by an area $\geq$ 1000 m^2, maximum source power $\geq$ 25 kW or source heat extraction $\geq$ 50 MWh/y. Hereby, entire building sites can be provided with heating and cooling energy. By combining LSCs and low-temperature district heating networks, this type of heat supply can be used not only in rural regions but also in densely inhabited areas. The district heating and cooling networks operate with low system temperatures in the range of very shallow subsurface temperatures, resulting in very low heat losses [2–4]. Furthermore, the network itself can gain up to 50% of the heat demand [2].

Such a combination is being studied in detail scientifically as part of the KNW-Opt research project (Grant No. 03EN3020C). On this test site, which is located at Bad Nauheim in Hesse in the centre of Germany, a two-layer LSC with a total area of 22,000 m^2 was placed beneath an agricultural area. The collectors are installed at a depth of 1.5 and 3.0 m below

ground level (m b. g. l.). A new residential settlement is supplied via a low-temperature district heating and cooling network.

1.2. Determination of Thermal Conductivity of Soils

Exploring the subsurface, especially its thermal properties, is necessary for several reasons in the context of LSCs. Thermal soil parameters are crucial for the design, performance and as input parameters for the modelling of horizontal systems [5–9]. Furthermore, the effects of heat and cold extraction on the subsurface for water law and ecological considerations can also be estimated more realistically. Such considerations particularly concern the saturated zone, as thermal changes can result in hydrochemical and biological alterations of groundwater [10–13]. Therefore, a monitoring concept can be used to ensure the sustainable application of larger shallow geothermal systems [14,15]. Furthermore, the unsaturated zone and its thermal properties are essential, as the groundwater temperature down to a depth of 10 to 15 m is mainly influenced by vertical heat transport [16]. In addition, the collectors are often located in the unsaturated zone due to the very shallow installation depth.

The main transport mechanism for heat in the unsaturated subsurface is conduction [17]. For this reason, the geothermal potential in the context of LSCs can be described by the thermal conductivity of soil (λ) [18]. This parameter depends on further soil properties such as water content, bulk density, soil texture and organic matter [17–20]. Based on these correlations, several models were created to calculate λ [21–24]. Furthermore, thermal conductivity can be measured directly, e.g., using a single-needle sensor [25–27]. However, this can only be conducted on a laboratory scale or in situ selectively on a small scale. For borehole heat exchangers in particular, thermal response tests (TRTs) are often used as an in situ measurement method [28,29].

Large-scale investigations are associated with increased effort. Since large-scale considerations are particularly required in the context of LSCs, an alternative determination of thermal conductivity on a larger scale would be more expedient. One potential approach could be non-invasive electrical resistivity tomography (ERT) and the derivation of soil parameters over longer distances and thus larger areas.

The methodology of geoelectrical measurements has developed significantly in recent decades and can be used to investigate the geophysical parameters on many different issues [30–33]. Because the physical parameters of soil which determine thermal conductivity are also decisive for the electrical resistivity and respective electrical conductivity (σ) in soils [34–36], a geothermal assessment performed by using geoelectrical measurements can be possible. Similar to thermal conductivity, σ is determined mainly by the parameters water content, density and organic content [37–41], although water content is more decisive as a single parameter [42]. Due to this correspondence, there are various attempts to derive thermal conductivity from electrical conductivity [35,36,42–46]. However, a direct dependency across all soil types is not present, which is why direct derivations often cannot be applied in a generalised manner [42,47]. For this reason, Schwarz and Bertermann [42] presented an indirect but generally applicable determination of thermal conductivity by ERTs for unsaturated soils.

1.3. Aims of This Study

This study aims to compare measured and derived thermal conductivities in the unsaturated soil zone of the LSC in Bad Nauheim. It is common practice to measure the thermal conductivity in situ or on a laboratory scale, e.g., using a single-needle sensor measuring device. Therefore, two different measurement methods on a laboratory scale are compared using samples from Bad Nauheim to work out their benefits and disadvantages.

A large-scale determination of thermal parameters in the subsurface—as it is required in the context of LSCs—can only be guaranteed by a very high number of measurements. For this reason, this study also examines the potential of deriving crucial physical and thermal soil parameters by ERTs according to Schwarz and Bertermann [42] and compares

the derived values with actual measurement results. ERTs could be an alternative method for performing large-scale thermal explorations of the unsaturated zone for corresponding projects. Moreover, this approach would be non-invasive and could also be applied after installing the LSC and refilling the collector area.

2. Materials and Methods

2.1. Test Site and Geological Conditions

Bad Nauheim is a city located at the eastern edge of the Taunus Mountain range. For subsurface exploration and sampling from 2019 to 2021 trial pits (TP) were conducted and boreholes (B), as well as ramming cores (RCD), were drilled. The location of the sampling points is shown in Figure 1a.

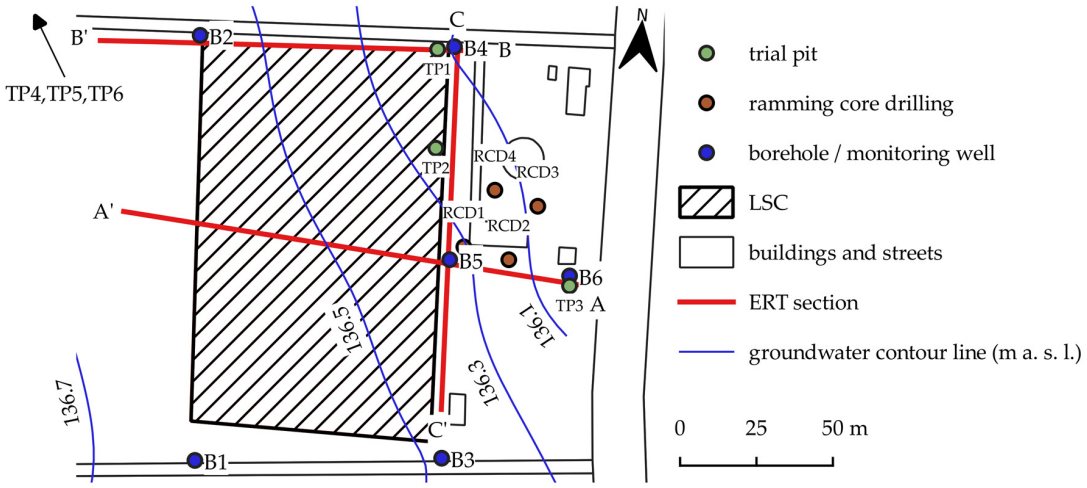

(**a**)

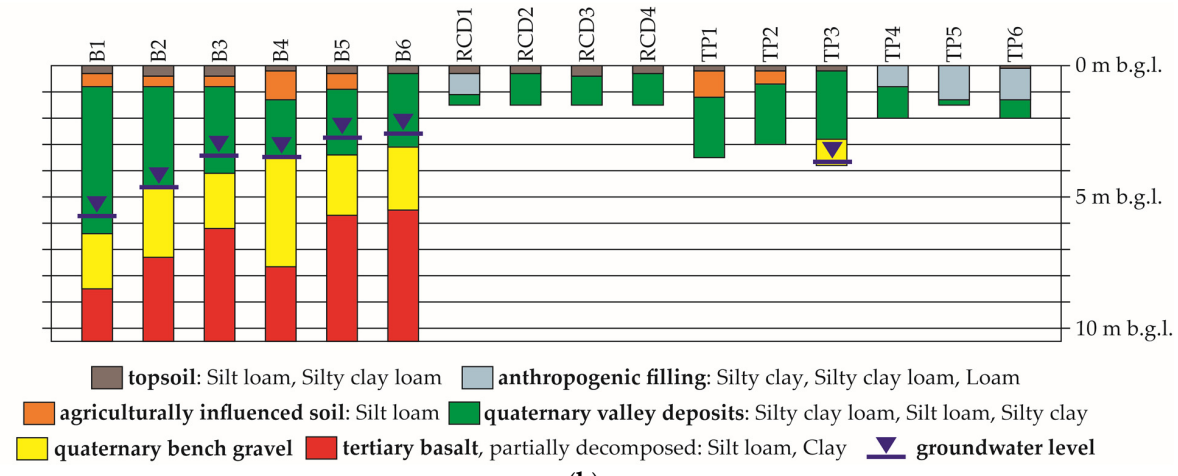

(**b**)

Figure 1. (**a**) Test site and location of sampling points, electrical resistivity tomography (ERT) sections and groundwater contour lines from the groundwater level measurements on 7 April 2021 specified in meters above sea level (m a. s. l.); (**b**) Boreholes (B1–B6), ramming core drillholes (RCD1-RCD4) and trial pits (TP1–TP6), thickness of their stratigraphic units in meters below ground level (m b. g. l.) and USDA (U.S. Department of Agriculture) soil classification for predominantly fine-grained soils based on grain size analyses. The groundwater level measured on 7 April 2021 and for TP3 on 25 November 2020 is also shown. TP2, TP4, TP5 and TP6 were conducted in backfilled areas, so that the stratigraphic layer structure may be disturbed, and the stratification shown above can only be understood as rough.

TP2 was conducted directly in the collector field and after backfilling with excavated material. Six 10.5 m deep boreholes for groundwater monitoring wells were installed around the LSC [14]. In addition, three more trial pits (TP4, TP5, TP6) were performed in the range of the low-temperature district heating network 170 to 300 m northwest of the LSC. Figure 1b shows the stratigraphic units encountered and their thickness at the various sample points.

At the test site, quaternary loamy valley deposits and bench gravels are present in the shallow subsurface [48]. These are overlain by topsoil and locally by agriculturally influenced soil and anthropogenic loamy fillings, which are predominantly redeposited or anthropogenically influenced valley deposits or similar soil types. Several grain size analyses were performed for the exclusively fine-grained soils (Figure 1b). Towards the gravel aquifer layer boundary, the gravel content already increases in the quaternary loam. The underlying bench gravel is the local shallow aquifer. The groundwater flow direction is to the northeast and east towards the river Usa. (Figure 1a). The bench gravel is followed by a very heterogeneous layer of tertiary basalt. The basalt largely decomposed to clayey silt with clay sections or clay known as 'Rotlehm' [49]. Deeper, the basalt layer gets more permeable because of its rising hard rock characteristics.

2.2. Field and Laboratory Investigations

2.2.1. Geotechnical and Soil Scientific Investigations

For the thermal evaluation of the subsurface, various field and laboratory investigations of crucial soil parameters were performed. A list is shown in Table 1. For this purpose, the trial pits and boreholes shown in Figure 1, and samples taken from them, were used. Water content determinations were performed in boreholes B2 to B6 and in TP2 to TP6, density determinations in TP1 to TP6. In addition, bulk density and water content measurements were conducted on the topsoil and the very near-surface valley deposits at eight locations in the range of the LSC or the immediate vicinity.

Table 1. Conducted field and laboratory investigations of soils and soil samples in the unsaturated zone in the range of the large-scale geothermal collector system (LSC) and the near low-temperature district heating and cooling network.

Parameter	Number of Tests	Method
dry bulk density (ρ_b)	36	undisturbed sampling with stabbing cylinders and oven drying based on DIN EN ISO 11272 [50]
gravimetric water content (ω)	57	sampling and oven drying based on DIN EN ISO 17892-1 [51]
Atterberg limits and plasticity index	5	plastic limit (ω_P), liquid limit (ω_L) and plasticity index (I_P) according to DIN EN ISO 17892-12 [52] and shrinkage limit (ω_S) according to Krabbe [53]

The trial pits were opened to a maximum of 3.4 m b. g. l., so undisturbed sampling was not possible at a deeper level. For the large-scale determination of the bulk density (ρ_b) for the depths 0.5 to 3.5 m b. g. l. in 0.5 m intervals, the average value was calculated using measured values in the range $\pm$0.5 m from the corresponding depth. Due to the similar soil types and stratigraphic units, the results of the more distant TP4, TP5 and TP6 were also considered for a large-scale approach, which includes the low-temperature district heating network. For the depths 4.0 m to 5.0 m b. g. l., the average value calculated for 3.5 m b. g. l. was also simplified assumed. However, this only applies to the areas of the test site where unsaturated quaternary loam is still present at this depth and not the coarse bench gravel.

In accordance with the procedure for ρ_b, the average value of the gravimetric water content (ω) was calculated for the depth steps between 0.5 and 5.0 m b. g. l.

The average depth-dependent values of ρ_b and ω were used to calculate the volumetric water content (θ) considering the density of water (ρ_w) as follows:

$$\theta = (\omega \cdot \rho_b)/\rho_w \quad (1)$$

2.2.2. Thermal Conductivity Measurements on a Laboratory Scale

To determine the thermal conductivity of soils in the unsaturated zone on a laboratory scale, two methods were used. The procedures and the measuring devices for these two methods are described in Table 2 and schematic in Figure 2. The evaporation method is based on the procedure described by Markert et al. [27].

Table 2. Measurement devices and approaches for thermal conductivity (λ) measurements with single-needle sensors on fine-grained, repacked soil samples. Thermal properties analyzer KD2Pro by Decagon Devices, Inc. and Tempos by METER Group, Inc.

Method	Thermal Properties Analyzer	Single-Needle	Accuracy	Measuring Interval	Preparation/Experimental Procedure
Evaporation	KD2 Pro Tempos	TR-1 (10 cm); TR-3 (10 cm)	±10% from 0.2–4.0 W/(m·K); ±10% from 0.1–4.0 W/(m·K)	15 min-days	• Installation of oven dried and mortared soil sample in measuring cylinder • Capillary saturation • Continuous or temporary measurement of λ with decreasing water content due to evaporation [27] • Additional measurement after oven drying
Punctual	Tempos	TR-3 (10 cm)	±10% from 0.1–4.0 W/(m·K)	-	• Installation of mortared soil samples in measuring cylinder at two selected medium water contents (ω_1 and ω_2) • Measurement of λ at ω_1 and ω_2 • Additional measurements after oven drying (ω_{dry}) and capillary saturation (ω_{sat})

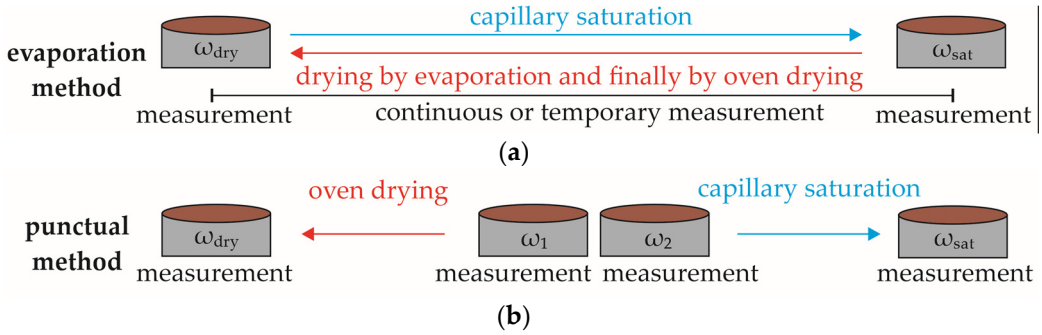

Figure 2. Schematic illustration of the procedure for thermal conductivity (λ) measurements explained in Table 2 with (**a**) evaporation method based on Markert et al. [27] and (**b**) punctual method with measurement of λ at four selected gravimetric water contents (ω): medium water contents (ω_1 and ω_2), water content after oven drying (ω_{dry}) and water content after capillary saturation (ω_{sat}). The selection of the water contents ω_1 and ω_2 was based on the results of the evaporation method.

The dimensions of the used single-needle TR-1 and TR-3 sensors comply with the specifications according to IEEE Std 442-1981 [54] and ASTM D5334 [55]. The volumes of measuring cylinders were 397 cm^3 and 944 cm^3. After oven drying (65 °C), the measurements were performed after the samples had cooled down to room temperature. For each measurement, the weight and water content of the sample was recorded.

Each measurement at a certain water content of the punctual method is an average of three measured values, which deviate from each other by a maximum of 0.1 W/(m·K). In the case of sample TP4 0.6 m b. g. l, only two values were used for the measurement at ω_{sat}.

In addition, changes of ρ_b for selected measurements with the evaporation method were documented, since swelling and shrinkage of the samples were observed.

A list of the samples and sample configurations on which thermal conductivity measurements were performed is shown in Table 3.

Table 3. Soil samples, with sampling depth in meters below ground level (m b. g. l.) and USDA (U.S. Department of Agriculture) soil classification, on which thermal conductivity measurements were performed. In addition, the bulk density (ρ_{b_ini}) with which the soil sample was initially installed in the measuring cylinder is shown. By installing the sample twice with the punctual method, ρ_{b_ini} can also differ slightly within the test.

Sampling Point	Depth [m b. g. l.]	Stratigraphic Unit	USDA	Evaporation Method	Punctual Method	ρ_{b_ini} [g/cm^3]
B2	4.0–4.6	Quaternary valley deposits	Silty clay loam	✓	✓	1.48; 1.45; 1.46
B4	8.0–9.0	Tertiary basalt (Rotlehm)	Clay	✗	✓	1.27; 1.38
B5	6.2–6.9	Tertiary basalt (decomposed)	Silt loam	✗	✓	1.43; 1.46
TP1	0.2	Topsoil	Silt loam	✓	✗	1.57
	1.4–1.9	Quaternary valley deposits	Silty clay loam	✓	✗	1.39
	2.4	Quaternary valley deposits	Silt loam	✓	✗	1.47
	2.9–3.4	Quaternary valley deposits	Silt loam	✓	✗	1.50
TP2	0.2	Topsoil	Silty clay loam	✗	✓	1.22; 1.24
	0.7	Agriculturally influenced soil	-	✗	✓	1.15
	1.4	Quaternary valley deposits	Silt loam	✓	✓	1.16; 1.15
	1.9	Quaternary valley deposits	-	✗	✓	1.36
	2.4	Quaternary valley deposits	-	✓	✓	1.50; 1.47; 1.49
	2.9	Quaternary valley deposits	Silt loam	✗	✓	1.55; 1.56
TP4	0.6	Anthropogenic filling	Silty clay	✗	✓	1.41; 1.49
	1.2	Quaternary valley deposits	Silty clay loam	✗	✓	1.47; 1.55
	1.6	Quaternary valley deposits	Silt loam	✓	✓	1.51; 1.50
TP6	0.6	Anthropogenic filling	Loam	✗	✓	1.28; 1.29
	0.6	Anthropogenic filling	Loam	✗	✓	1.28; 1.29
	1.6	Quaternary valley deposits	Silty clay loam	✓	✓	1.30; 1.28

For the determination of the depth-dependent, large-scale thermal conductivity, λ was calculated for specific depth intervals using regressions with a second-degree polynomial function of corresponding measurement results and the average, depth-dependent values of ω. The two measurement methods were considered separately.

For the evaporation method, only one measurement point per 24 h is used for the thermal conductivity calculation and illustration in the following. This results in the single measurement at ω = 0.0 g/g being weighted more for the regression. Due to the similar soil types and stratigraphic units, the results of the more distant TP4 and TP6 were also considered for a large-scale approach, which includes the near low-temperature district heating network.

2.3. Electrical Resistivity Tomography (ERT) and Parameter Derivation

Along three 2D sections, ERTs were performed on the test site on 7 April 2021, i.e., after refilling the collector field. The sections partly crossed groundwater monitoring wells to compare the results with the layer structure of drilling profiles and the measured groundwater levels (Figure 1a).

The measurements were taken at a frequency of 4.16 Hz with the earth resistivity meter 4point light by LGM—Lippmann Geophysical Equipment and the software GeoTest (version 2.4.3) by Geophysics—Dr. Rauen. Methodology and measurement configuration

for each section is shown in Table 4. A total of 80 electrodes were used for Section A and 60 electrodes for Sections B and C.

Table 4. Methodology and measurement configuration of electrical resistivity tomography (ERT) for Sections A, B and C.

Section	Method	Maximal Measurement per Point	Threshold Measurement Error [%]	Electrode Spacing [m]	Length [m]	Measured Layers	Measured Depth [m b. g. l.]
A	Wenner array [31]	40	0.1	2	158	20	28
B		25	0.2	2	118	17	20
C		25	0.2	2	118	17	20

For data processing, the measured pseudo-resistivities were inverted using the software Res2DInv (version 4.03.36) by Aarhus GeoSoftware. Since the terrain is slightly sloping, an elevation profile was implemented. The calculation was performed using the robust inversion settings and the full Gauss–Newton method. To generate smoother resistivity transitions, the calculated cells were halved by using the halved-unit electrode spacing option. The values of the 10th iteration of inversion processes were considered for the evaluation. Section A showed an error of 3.8%, Section B 1.4% and Section C 2.1%.

The derivation of λ is performed as described by Schwarz and Bertermann [42]. This approach is based only on the electrical conductivity σ_T, which is corrected by temperature factor f_T according to Sheets and Hendrickx [56] to electrical conductivity at a temperature of 25 °C (σ_{25}):

$$\sigma_{25} = f_T \cdot \sigma_T \quad (2)$$

$$f_T = 0.4470 + 1.4034 \cdot e^{-T/26.815} \quad (3)$$

For the temperature correction, the average value of all temperature monitoring stations located at B1–B6 of the measurement on 22 April 2021 was formed, in this case T = 10.1 °C [14]. The electrical conductivity σ_T is the reciprocal value of the measured electrical resistivity (ER).

For the derivation of λ, several steps are required in this approach. First, θ is calculated according to Bertermann and Schwarz [57] considering correction factors for the soil type groups Clay (X_{clay}) and Silt (X_{silt}) according to Schwarz and Bertermann [42]:

$$\theta = e^{0.3415 \cdot \ln(\sigma_{25}) + 4.228} - X_{\text{clay or silt}} \quad (4)$$

$$Xclay = -34.122 \cdot \sigma 25 + 5.1063 \quad (5)$$

$$Xsilt = -204.75 \cdot \sigma 25 + 5.2482 \quad (6)$$

The soil texture groups are also defined by σ_{25} in three different ranges (Sand: <0.01 S/m; Silt: 0.01–0.05 S/m; Clay: >0.05 S/m). These separation ranges are used to determine the selection of the respective correction factor for θ as well as for the calculation of ρ_b. Bulk density is derived as follows:

$$\rho_{b\_clay} = 0.9565 \cdot \sigma_{25} + 1.1683 \quad (7)$$

$$\rho_{b\_silt} = 4.6015 \cdot \sigma_{25} + 1.3362 \quad (8)$$

$$\rho_{b\_sand} = 1.4 \quad (9)$$

By deriving θ and ρ_b, the thermal conductivity can be calculated. As proposed by Schwarz and Bertermann [42], the calculation in this study is performed according to Kersten [22]:

$$\lambda = 0.1442 \cdot \left(0.7 \cdot \log\left(\frac{\theta}{\rho b}\right) + 0.4\right) \cdot 10^{0.6243 \cdot \rho b} \quad (10)$$

The inverted electrical resistivities and the thermal conductivities derived from them were interpolated with the Surfer® mapping software by Golden Software and illustrated graphically.

For the comparison of the derived parameters with measured values, the average values of ρ_b, θ and λ per measured layer for each section were calculated.

3. Results

3.1. Bulk Density and Water Content

The measured average values for ω and ρ_b and the calculated volumetric water contents using Equation (1) are listed in Table 5.

Table 5. Average bulk densities (ρ_b) and gravimetric water contents (ω), which were determined in the unsaturated zone, and with Equation (1) calculated average volumetric water contents (θ). The standard deviation and the number of measured values used in each case are also shown in the brackets. For the depths 4.0 m to 5.0 m b. g. l., the average ρ_b calculated for 3.5 m b. g. l. is also assumed in a simplified way.

Depth [m b. g. l.]	ω [g/g]	ρ_b [g/cm^3]	θ [cm^3/cm^3]
0.5	0.17 (0.06/24)	1.46 (0.16/19)	0.24
1.0	0.18 (0.06/23)	1.40 (0.15/12)	0.25
1.5	0.22 (0.04/16)	1.45 (0.16/11)	0.32
2.0	0.21 (0.05/17)	1.43 (0.09/8)	0.29
2.5	0.19 (0.04/8)	1.53 (0.10/5)	0.28
3.0	0.17 (0.05/11)	1.59 (0.07/3)	0.28
3.5	0.16 (0.05/6)	1.59 (0.00/1)	0.25
4.0	0.15 (0.04/7)	1.59 (-/-)	0.24
4.5	0.17 (0.04/3)	1.59 (-/-)	0.27
5.0	0.12 (0.05/3)	1.59 (-/-)	0.19

The water content and bulk density showed location-dependent fluctuations, especially in the area very close to the surface. Water contents of 0.06 to 0.32 g/g were measured over the entire depth. The average water content initially increased with depth and decreased again from 2.0 m b. g. l. onwards.

Bulk densities between 1.2 and 1.7 g/cm^3 were measured. The average values were initially approximately constant and increased from 2.0 m b. g. l. downwards and are simplified and assumed to be constant from 3.5 m b. g l.

3.2. Atterberg Limits and Plasticity Properties

Table 6 shows the determined Atterberg limits and the plasticity index for soil samples examined. As can be seen, the shrinkage limit (ω_S) for four out of five samples was between 0.17 g/g and 0.19 g/g and the liquid limit (ω_L) between 0.28 g/g and 0.29 g/g. Only the sample from TP1 at 1.4–1.9 m b. g. l. showed a significantly higher liquid limit of 0.40 g/g and a lower shrinkage limit of 0.14 g/g. Thus, according to the ISSCS (Indian Standard Soil Classification System) plasticity chart, this sample is classified as intermediate plastic clay (CI). The remaining samples are classified as low plastic clays (CL), with plasticity indexes between 0.08 and 0.10.

3.3. Thermal Conductivity Measurements Using Evaporation Method

Thermal conductivities measured with the evaporation method are shown in Figure 3.

Table 6. Results of the determination of the liquid limit (ω_L), plasticity limit (ω_P), plasticity index (I_P) and shrinkage limit (ω_S), as well as the soil class determined from the ISSCS plasticity chart (PC): CI = intermediate plastic clay, CL = low plastic clay.

Sample Point	Depth [m b. g. l.]	ω_L [g/g]	ω_P [g/g]	I_P	ω_S [g/g]	PC
B2	2.7–4.6	0.29	0.19	0.10	0.17	CL
TP1	1.4–1.9	0.40	0.19	0.21	0.14	CI
TP1	2.9–3.4	0.29	0.21	0.08	0.19	CL
TP2	2.9	0.29	0.20	0.08	0.18	CL
TP4	1.6	0.28	0.21	0.08	0.19	CL

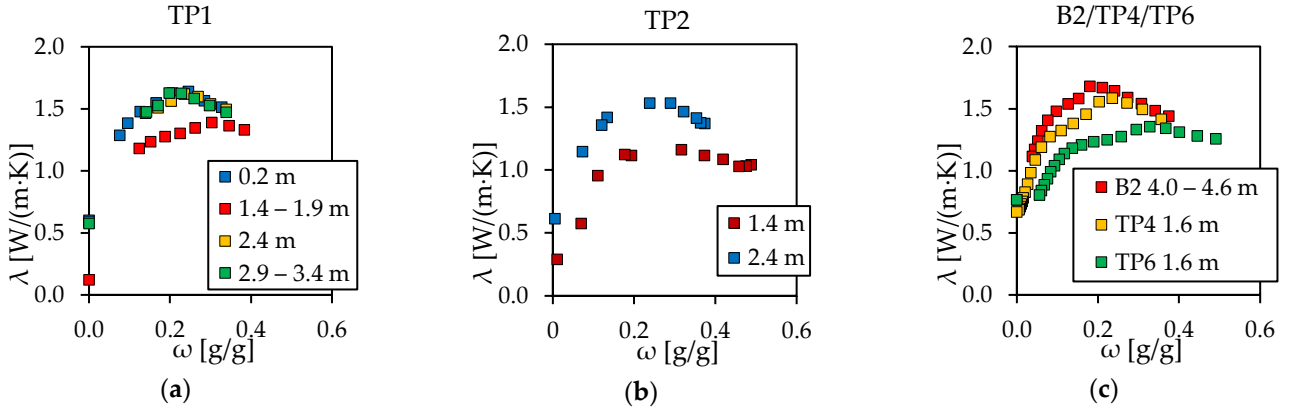

Figure 3. Results of thermal conductivity (λ) measurements as a function of the gravimetric water content (ω) using the evaporation method for samples of (**a**) TP1, (**b**) TP2 and (**c**) B2, TP4 and TP6. A maximum of one measuring point per 24 h is displayed.

The measurements initially showed increasing values of λ with decreasing ω. The thermal conductivity reached a maximum and decreased again as the water content continued to decrease. The differences between the maximum thermal conductivity and the thermal conductivity at saturated conditions were between 0.1 and 0.3 W/(m·K). Maximum values for λ between 1.2 and 1.7 W/(m·K) were measured.

Furthermore, changes in the volume of the samples were observed during saturation, and drying due to evaporation. At selected samples those changes were recorded. The results are summarised in Table 7.

Table 7. Observed bulk density changes during saturation and drying using the evaporation method: ρ_{b_ini} = initially installed bulk density, ρ_{b_sat} = bulk density after saturation, ρ_{b_dry} = bulk density after oven drying. Due to the not completely straight surface of the soil body after swelling and shrinking, the indication of ρ_{b_sat} and ρ_{b_dry} is kept rough.

Sample Point	Depth [m b. g. l.]	ρ_{b_ini} [g/cm^3]	ρ_{b_sat} [g/cm^3]	ρ_{b_dry} [g/cm^3]	Clay Content
TP2	1.4	1.16	~1.2	~1.5	26%
TP2	2.4	1.50	~1.3	~1.6	24% [1]
TP4	1.6	1.51	~1.4	~1.7	23%
TP6	1.6	1.30	~1.2	~1.6	35%
B2	4.0–4.6	1.48	~1.3	~1.8	35%

[1] Clay content linearly interpolated between the determined values at 1.4 m and 2.9 m b. g. l.

Accordingly, significantly lower bulk densities after saturation and significantly higher bulk densities after drying in comparison to the initially installed bulk density (ρ_{b_ini}) were observed. During the test procedures, alterations of ρ_b by amounts of 0.3 g/cm^3 to 0.5 g/cm^3 occurred.

3.4. Thermal Conductivity Measurements Using Punctual Method

The results of the punctual method are shown in Figure 4. The water contents to be measured were based on the results of the evaporation method. However, it turned out that significantly lower maximum values of ω were achieved due to saturation. As a result, the measurements at ω_2 and ω_{sat} were partially conducted at similar water content values.

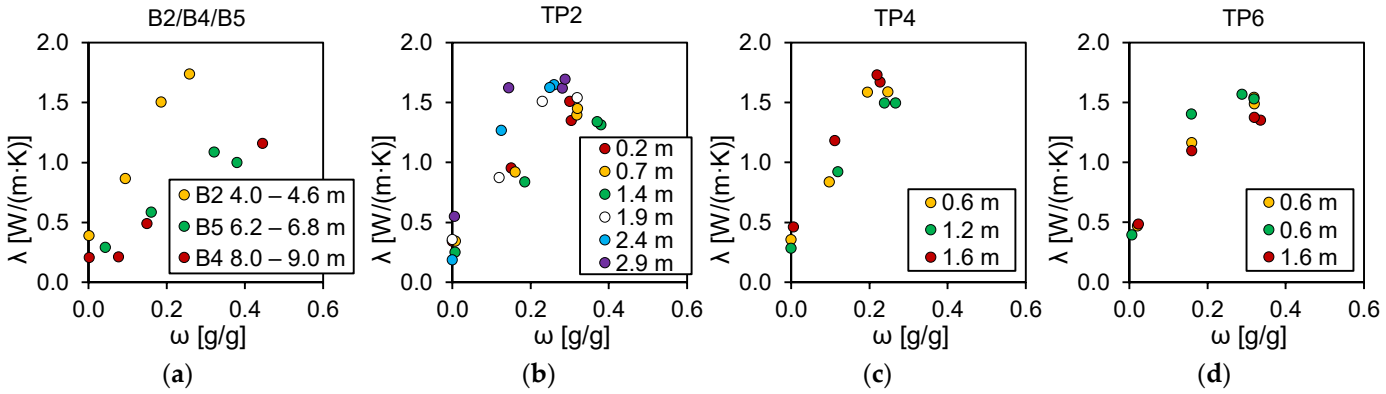

Figure 4. Results of thermal conductivity (λ) measurements as a function of the gravimetric water content (ω) using the punctual method for samples of (**a**) B2, B4 and B5, (**b**) TP2, (**c**) TP4 and (**d**) TP6.

Here, predominantly increasing thermal conductivities occurred with increasing ω. Maximum values for λ between 1.3 W/(m·K) and 1.7 W/(m·K) were achieved for quaternary valley deposits or overlaying layers.

3.5. Depth-Dependent Thermal Conductivities

The measured values for λ, sorted by the depth interval from which the respective soil samples were taken and by measurement method, are shown in Figure 5.

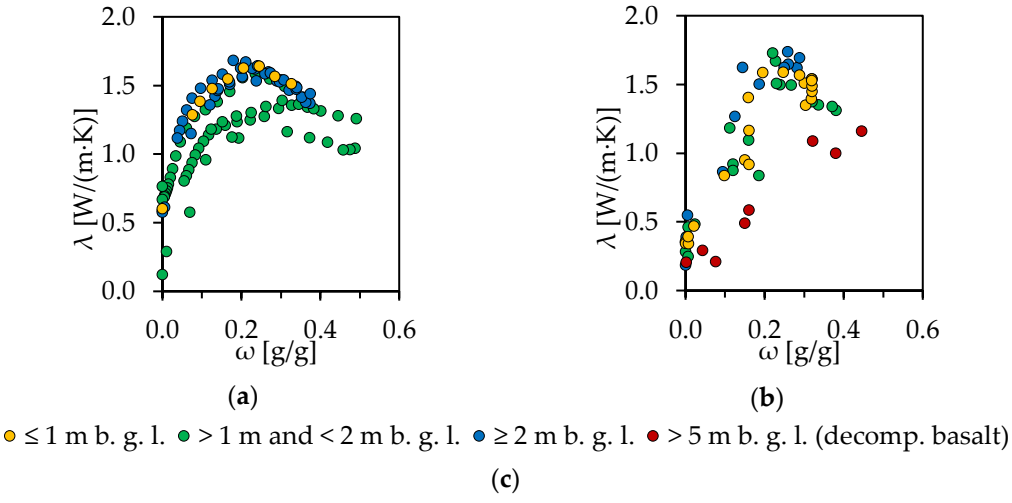

Figure 5. Measured values for λ as a function of gravimetric water content in specific depth intervals for (**a**) the evaporation method and (**b**) the punctual method. In addition, the measured thermal conductivity of decomposed basalt samples (>5 m b. g. l.) is shown in (**b**). For the evaporation method, a maximum of one measuring point per 24 h is displayed. Chart legend is shown in (**c**).

The depth-dependent thermal conductivities were calculated with the gravimetric water contents listed in Table 5. For this purpose, a regression of the measurement results with a second-degree polynomial function for each depth interval was used. The results are shown in Table 8. The quality of the regression is determined by the coefficient of determination (R^2) and Root Mean Square Error (RMSE).

By using a regression based on ω, the results are considered independently of bulk density. Furthermore, due to the density changes during the evaporation method, a determination of the volumetric water content is not possible.

Table 8. Thermal conductivity per depth step using regression with a second-degree polynomial function as a function of the gravimetric water content for the evaporation method ($\lambda_{evaporation}$) and the punctual method ($\lambda_{punctual}$). The quality of the respective regression is shown in the form of the coefficient of determination (R^2) and Root Mean Square Error (RMSE).

Depth [m b. g. l.]	$\lambda_{evaporation}$ [W/(m·K)]	$R^2_{evaporation}$/RMSE	$\lambda_{punctual}$ [W/(m·K)]	$R^2_{punctual}$/RMSE
0.5	1.6	0.98/0.04	1.2	0.93/0.13
1.0	1.6		1.3	
1.5	1.4	0.73/0.16	1.4	0.87/0.17
2.0	1.6	0.90/0.09	1.6	0.95/0.12
2.5	1.6		1.5	
3.0	1.6		1.5	
3.5	1.5		1.4	
4.0	1.5		1.4	
4.5	1.6		1.5	
5.0	1.4		1.3	

With the punctual method, between three and five samples were measured per depth interval. For the evaporation method, one measurement for the depth $\leq$ 1 m b. g. l. was performed. Four measurements were conducted for each of the remaining depth levels.

3.6. ERTs and Parameter Derivation

The measured and interpolated electrical resistivities for each section are shown in Figure 6. In the quaternary valley deposits, as well as in the overlaying layers, electrical resistivities between 20 and 40 Ω·m were mostly observed. Section C showed locally higher resistivities, which, however, are due to distribution shafts. The boundary to the adjacent bench gravel, which also approximately represents the groundwater level, was characterised by increasing resistivities. In the aquifer, values for ER between 40 and 100 Ω·m were measured, whereby even higher values can be explained by distribution shafts in Section C. The decomposed basalt closer to the surface showed similarly high values, in deeper layers ER decreased to values between 0 and 20 Ω·m.

For the derivation of soil parameters from ER and respectively σ_{25}, only the unsaturated subsurface was considered in the following. On 7 April 2021, the average groundwater level was 136.3 (±0.3) m above sea level. After temperature correction (Equation (2)), the electrical conductivities predominantly showed values in the separation range of the silt and clay soil type groups.

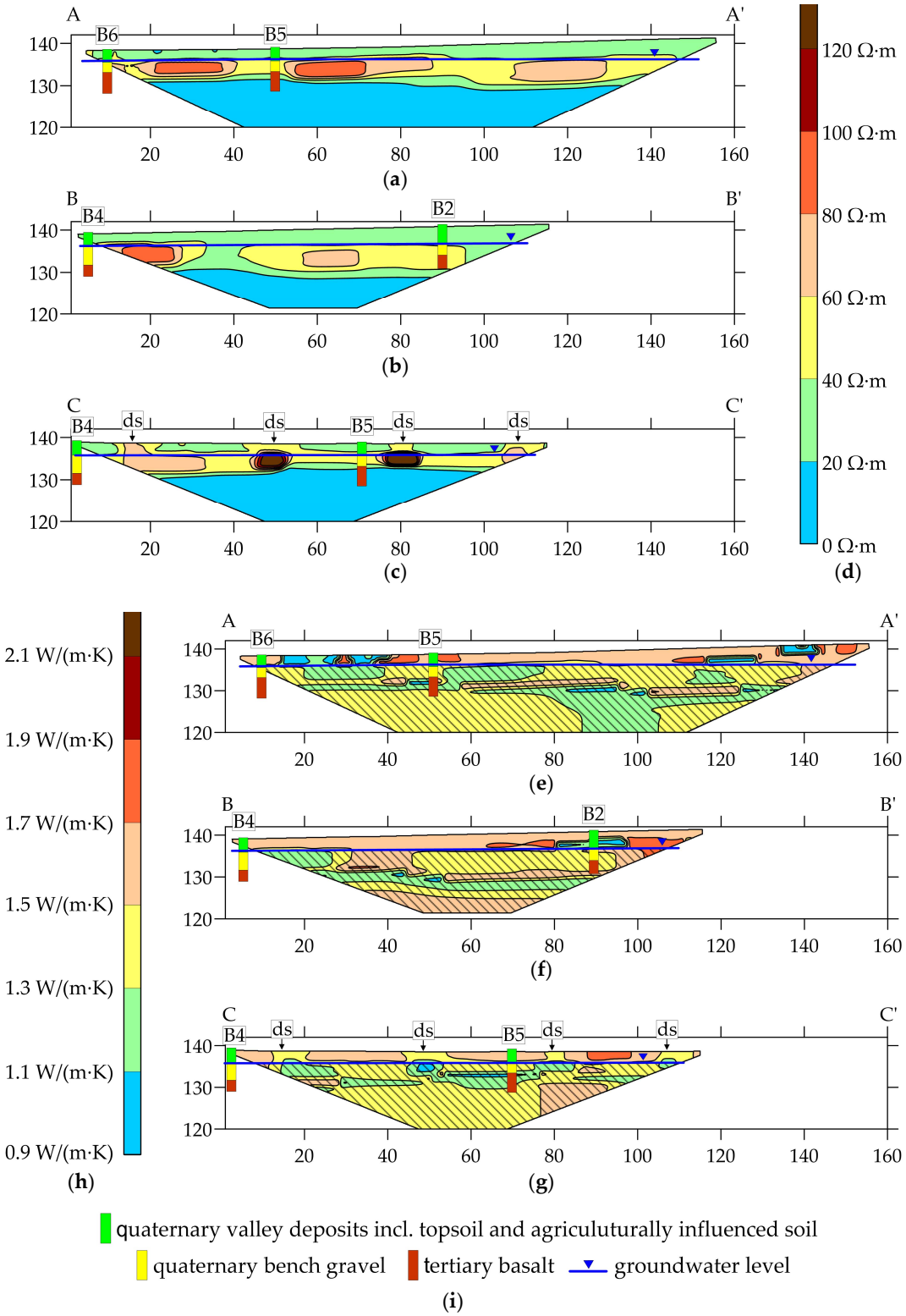

Figure 6. (**a**–**d**) Distribution of electrical resistivities in the subsurface along the ERT sections with colour scale; (**e**–**h**) derived thermal conductivities for each ERT section with colour scale. The derivation method is only applicable to the unsaturated zone (area that is not hatched). Shown also are simplified profiles of boreholes crossed by ERT sections and groundwater level from 7 April 2021, legend is shown in (**i**). In addition, the location of distribution shafts (ds) is shown in Section C. Altitudes are given in meters above sea level, length in meters.

As can be seen in Table 9, the derived average bulk densities in the unsaturated zone differed only slightly between the individual sections and with depth, averaging 1.49 g/cm^3. It is similar to θ, with an average value of 0.25 cm^3/cm^3. The thermal conductivity ranged between 1.5 and 1.6 W/(m·K) over large ranges of the sections with locally limited deviations (Figure 6e–g). Especially in the first 50 m of Section A, significantly lower values between 0.9 and 1.1 W/(m·K) were observed. In Section C, lower values due to the distribution shafts were calculated.

Table 9. Average derived values for ρ_b, θ and λ for each section and for each measured layer of the ERTs. The standard deviation is also shown in the brackets.

Depth [m b. g. l.]	ρ_b [g/cm^3]			θ [cm^3/cm^3]			λ [W/(m·K)]		
	A	B	C	A	B	C	A	B	C
0.5	1.46 (0.13)	1.51 (0.01)	1.51 (0.03)	0.26 (0.02)	0.25 (0.01)	0.25 (0.03)	1.5 (0.2)	1.6 (0.0)	1.6 (0.1)
1.1	1.45 (0.13)	1.51 (0.01)	1.51 (0.03)	0.26 (0.02)	0.25 (0.01)	0.24 (0.03)	1.5 (0.3)	1.6 (0.0)	1.6 (0.1)
1.7	1.47 (0.13)	1.52 (0.01)	1.51 (0.03)	0.26 (0.02)	0.25 (0.01)	0.24 (0.03)	1.5 (0.2)	1.6 (0.0)	1.6 (0.1)
2.3	1.50 (0.09)	1.50 (0.09)	1.50 (0.03)	0.26 (0.02)	0.26 (0.02)	0.24 (0.03)	1.6 (0.2)	1.6 (0.2)	1.5 (0.1)
3.1	1.46 (0.12)	1.47 (0.12)	-	0.25 (0.04)	0.25 (0.03)	-	1.5 (0.3)	1.5 (0.2)	-
3.9	1.42 (0.15)	1.45 (0.15)	-	0.25 (0.03)	0.26 (0.02)	-	1.4 (0.3)	1.5 (0.3)	-
4.7	1.49 (0.00)	1.54 (0.01)	-	0.23 (0.00)	0.28 (0.01)	-	1.5 (0.0)	1.7 (0.0)	-

4. Discussion

4.1. Comparison of Laboratory-Scale Methods for Determination of Thermal Conductivity Using Single-Needle Sensors

In the process of the evaporation method, it was observed that maximum values of λ were reached at a medium water content and not at full saturation as expected (Figure 3). Alterations of ρ_b due to swelling and shrinkage of the sample in the measuring cylinder were also evident. Since, in addition to water content, bulk density also has a significant influence on λ [17–20], it is assumed that these density changes caused the observed correlation of thermal conductivity and ω.

The shrinkage and swelling processes due to water content changes in clayey soils are further known [58–60]. In simplified terms, soil shrinks with decreasing water content until the shrinkage limit [61] and then reaches the highest bulk density. However, the thermal conductivity maximum was reached when the optimum ratio of ρ_b and ω was present ($\omega \geq \omega_S$). The deviating correlation of λ and water content that occurred due to shrinkage is also described by Ardiansyah et al. [62].

The soil samples examined here showed a high (Pearson's coefficient r = 0.90) and significant (*p*-value = 4%) linear correlation between the extent of shrinkage and clay content (Figure 7a). However, the clay content is only a rough approach to estimating the susceptibility of soils for shrinkage, since shrinkage is a complex process and contains different phases [63]. In addition to the amount of clay, the type of clay minerals is also decisive [58]. As repacked samples were used, the disturbance of the structural stability due to the installation and compaction of the dried soil samples can also lead to a changed and potentially increased shrinkage behaviour [64]. Therefore, due to the predominantly low plasticity indexes, it is assumed that the repacking process also caused a significant proportion of the observed volume changes. Furthermore, the higher values of ρ_{b_dry} than those of ρ_{b_ini} also indicate that decreasing water contents additionally led to a rearrangement of the grain structure.

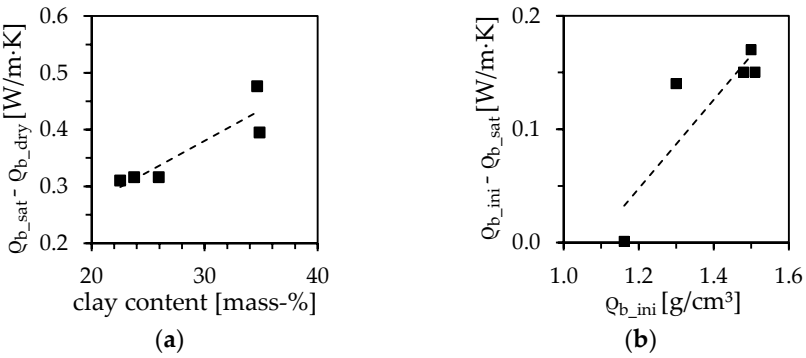

Figure 7. (**a**) Correlation of the difference of ρ_{b_sat} and the bulk density after oven drying (ρ_{b_dry}) with clay content; (**b**) correlation of the difference between the initial bulk density (ρ_{b_ini}) and the density after saturation (ρ_{b_sat}) with ρ_{b_ini}. The differences were calculated with the actual measured bulk densities and not with the rough indication of Table 7.

The amount of swelling during capillary saturation also showed a high (r = 0.88) and significant (*p*-value = 5%) linear correlation with the initially set bulk density (Figure 7b). Increased swelling behaviour with increasing originally-set density was observed.

Installing the soil in the measuring cylinder at a higher water content would reduce the effects of swelling of clayey soils. Similarly, by using undisturbed samples, increased shrinkage during drying, caused by the disturbance of structural stability, can be ruled out.

Both methods were performed on five identical samples, so the results can be compared (Figure 8a–e). The values for ρ_{b_ini} only differ by a maximum of 0.03 g/cm^3.

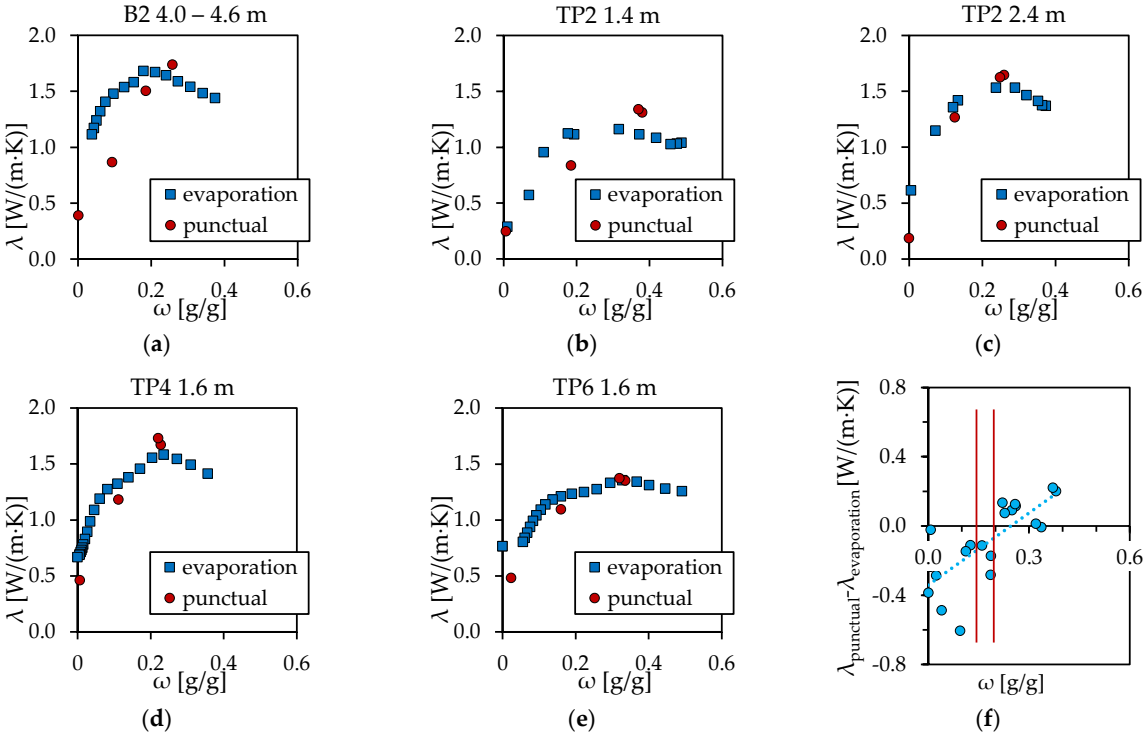

Figure 8. (**a**–**e**) Comparison of the results of the evaporation method and the punctual method. For the evaporation method, a maximum of one measuring point per 24 h is displayed; (**f**) correlation between the differences of measured values for λ with the punctual method ($\lambda_{punctual}$) and the evaporation method ($\lambda_{evaporation}$) at matching values of ω. The two red lines represent the area, where ω_S is located according to Table 6. If no measurement data was available at equal water contents, λ was linearly interpolated.

The measured values for λ differed by up to 0.6 W/(m·K) at equal water contents. These differences correlated clearly (r = 0.75) and significantly (*p*-value = 0%) with ω (Figure 8f). At low water contents ($\omega \leq \omega_S$), higher values for λ were measured with the evaporation method, whereas at higher water contents ($\omega > \omega_S$), higher values were determined with the punctual method. This can also be explained by the shrinking and swelling, and the resulting higher and lower densities which occur during the evaporation method. However, this is not always related to the extent of the density change and there were deviations from it.

The comparatively higher densities after capillary saturation also resulted in lower values for ω_{sat}. It is also assumed that in some cases complete saturation by capillary saturation was not achieved with the punctual method.

Due to low water content differences during capillary saturation and oven drying, swelling and shrinkage processes can be significantly reduced with the punctual method. In this study, ω_2 was often almost equal to ω_{sat}, and ω_1 was in the range of ω_S or below. Therefore, an approximately constant density is assumed for the measurements. The punctual method, therefore, has the benefit of a largely controlled and constant bulk density. However, compared to the evaporation method, a large amount of measuring points can only be achieved with increased effort in the laboratory by re-installing the sample each time.

Considering the calculated depth-dependent thermal conductivities (Table 8), the values of the evaporation method were particularly higher at 0.5 and 1.0 m b. g. l., by 0.1 W/(m·K) on average. As can be seen in Table 5, the used values of ω were between 0.12 and 0.22 and in the range of ω_S (Table 6). Accordingly, with the evaporation method, higher bulk densities between 1.3 g/cm^3 and 1.8 g/cm^3 can be assumed, with a positive effect on thermal conductivity [17–20]. With the punctual method values for ρ_b between 1.1 g/cm^3 and 1.6 g/cm^3 were used (Table 3). Thus, the actual bulk densities of the evaporation method were closer to the measured average bulk densities (Table 5), especially in the near-surface area, and, therefore, presumably provide more realistic values in a large-scale consideration including the near low-temperature district heating network.

At 1.5 m b. g. l., lower thermal conductivities were measured with the evaporation method compared to other depths, despite similar water contents. In addition, the lower value for R^2 showed a greater variation in measured values. It is assumed that the CI-soil partially present at this depth has different thermal properties and is less conductive than CL-soil occurring elsewhere (Table 6).

With this large-scale approach, it must be considered that water content and bulk density can be variable over a large area or seasonally due to different land use, climatic influences, or oscillating groundwater level. Accordingly, thermal conductivity is also a variable parameter.

As Figures 4 and 5 show, the decomposed basalt has lower thermal conductivities despite similar soil types and bulk densities. This can probably be attributed to the deviating mineralogical composition of this layer.

4.2. Derivation of Physical and Thermal Soil Parameters from ERTs

The measured electrical resistivities reflected the stratigraphic layer structure (Figure 6a–c). The loamy valley deposits and the loamy agriculturally- or anthropogenically-influenced soils showed already known resistivities for silt and loess loam [65]. Likewise, expectable values for water-saturated gravel were measured for the bench gravel layer. Here, the values fluctuated due to the different contents of fine-grained soil. Basalt as a hard rock normally has significantly higher electrical resistivities. However, low values of 30 Ω·m can also be measured in saturated basalt [66]. Especially in the deeper range, even lower values were observed here. These can be explained by the local decomposing to clayey 'Rotlehm', as in B4. In addition, the groundwater occurring in the partially decomposed and permeable basalt has high electrical conductivities, as was already measured in B3 [14] or is already known elsewhere in Bad Nauheim [67].

Figure 9 and Table 10 compare the Equations (2)–(10) derived soil parameters of the individual ERT sections (Table 9) with the measured averaged and calculated values of ρ_b, θ and λ listed in Tables 5 and 8.

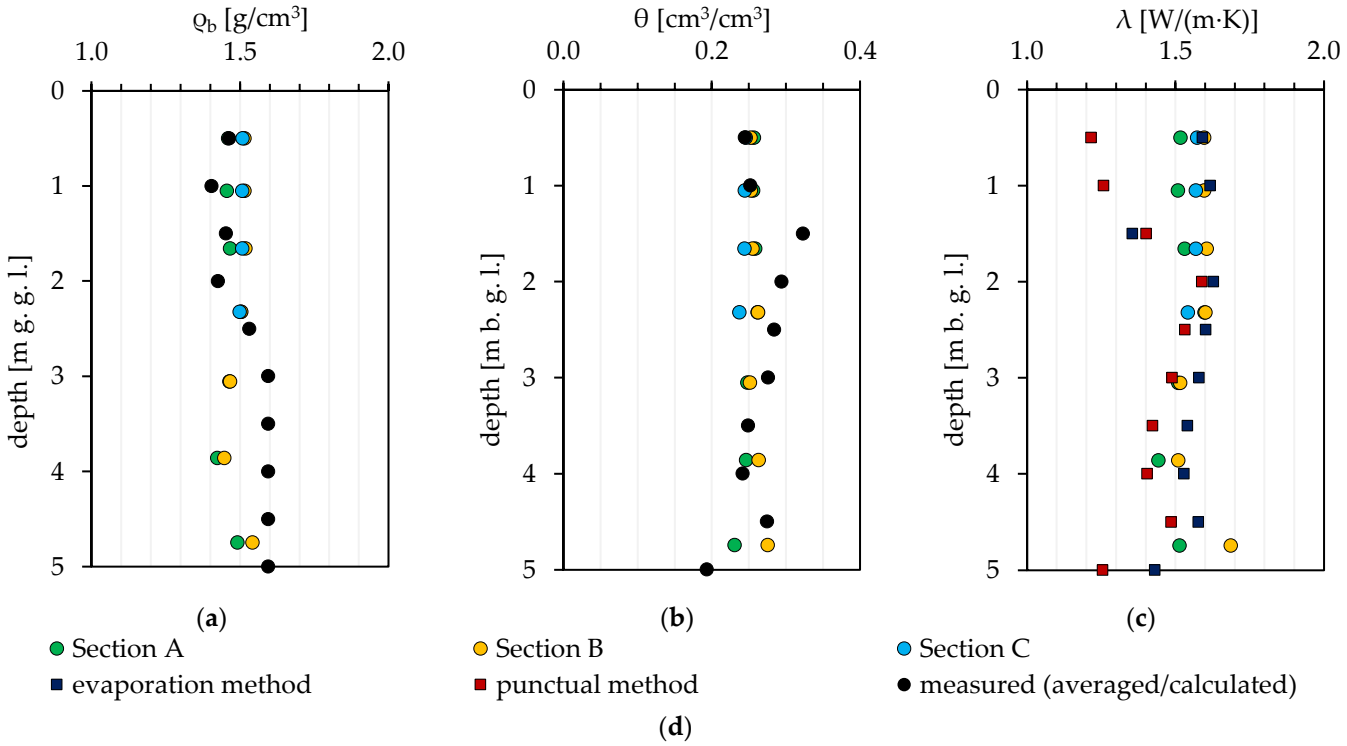

Figure 9. Comparison of average ERT-derived (**a**) bulk densities, (**b**) volumetric water contents and (**c**) thermal conductivities with measured and calculated values for the unsaturated zone. Chart legend is shown in (**d**).

Table 10. Deviations between measured or calculated soil parameters and from ERTs derived and averaged values for each section. For this, the derived values from the ERT were linearly interpolated for each depth step in intervals of 0.5 m from 0.5 m b. g. l. down to a depth of a maximum 4.5 m b. g. l. Negative values mean higher values derived from ERT.

Parameter	Minimum Deviation			Maximal Deviation			Average Deviation		
	A	B	C	A	B	C	A	B	C
ρ_b [g/cm³]	−0.1	−0.1	−0.1	0.2	0.1	0.0	0.1	0.0	−0.1
θ [cm³/cm³]	−0.01	−0.02	0.00	0.07	0.07	0.08	0.02	0.01	0.03
$\lambda_{punctual}$ [W/(m·K)]	−0.3	−0.4	−0.4	0.0	0.0	0.0	−0.1	−0.2	−0.2
$\lambda_{evaporation}$ [W/(m·K)]	−0.2	−0.2	−0.2	0.1	0.1	0.1	0.0	0.0	0.0

The average derived values of ρ_b and θ showed only minor deviations when compared with the average measured values. While the relationship between electrical conductivity and water content is significant, according to Schwarz and Bertermann [42], there is actually only a rough relationship between density and electrical conductivity. Therefore, especially the accuracy of the density derivation needs to be investigated in further studies.

Furthermore, as mentioned before, bulk density and water content can be locally and temporally variable. This is particularly evident from 0.5 to 1.5 m b. g. l. considering the calculated standard deviations (Table 5). For this reason, a comparison of only average values in largely uniform soil types is particularly appropriate. In addition, the local disturbances of electrical conductivities by the distribution shafts or other structures are in this case not very significant due to the use of average values.

The thermal conductivities derived from the ERTs were largely 1.5 and 1.6 W/(m·K) on average (Table 9). However, higher standard deviations (0.2–0.3 W/(m·K)) due to local sections with lower or higher values are given, especially for Section A and Section B. In total, there were no differences between the derived and measured values using the evaporation method on average. Only at a depth of 1.5 m b. g. l., derived values for λ were higher by 0.2 W/(m·K) in each section. This is probably due to the CI-soil present at this depth, which is not sufficiently resolved with the ERTs.

With the punctual method, the measured values were, on average, 0.1 W/(m·K) lower. The highest deviations (up to −0.4 W/(m·K)) were observed at 0.5 m b. g. l. and 1.0 m b. g. l., presumably due to the lower bulk densities used in the laboratory measurements. Over the entire depth of the unsaturated zone and considering both measurement methods, the average difference was −0.1 W/(m·K).

The use of average values along the ERT sections and of depth-dependent values for λ, determined from several laboratory scale measurements and water content measurements, provides a rough and large-scale comparison. This is considered particularly useful with regard to LSCs or other larger infrastructure projects. A small-scale comparison is not performed by this approach. Small and locally limited layers or areas with deviating thermal behaviour, such as the less-conductive CI-soil in this case, are not detected by this procedure. In addition, ERT sections can have locally small-scale, presumably unrealistic values due to interfering factors, either unknown or due to, for example, distribution shafts. These could decisively affect the derivation of soil parameters in detailed investigations.

5. Conclusions

The comparison of the two laboratory measurement methods using single-needle sensors—the evaporation method based on Markert et al. [27] and the punctual method—shows the benefits and disadvantages of both approaches.

With the evaporation method, changes in the density of the sample body affected the measurements. These swelling and shrinking processes were caused by the clay content and by the use of repacked soil samples. Such effects can be reduced by using undisturbed soil samples and by installing the soil sample in an already moist state. Soils with a low clay content are also expected to have fewer density alterations. The benefit of this method is that the continuous measurement generates a data set that can cover the complete water content range. In addition, the laboratory effort for each measurement is comparatively low.

With the punctual method, a sufficiently constant density can be ensured for the measurements—even with clayey and repacked soil samples. However, this is conditionally dependent on the selected water contents at which the thermal conductivity is measured. Due to the two times of installation in the measuring cylinders, the laboratory effort per measurement increases. In addition, it is only possible to generate a larger number of measurement points with greater effort or by combining both methods.

The thermal conductivities derived from the ERTs showed largely minor deviations from the laboratory measurements using a large-scale approach based on averaged values. According to the results of this study, ERTs could be used for non-invasive thermal exploration of the very shallow, unsaturated subsurface in the context of large-scale infrastructure projects such as LSCs. Due to the calculation of λ according to Kersten [22] as proposed by Schwarz and Bertermann [42], no prior knowledge about the subsurface to be investigated is required. However, the soil parameters derived in this study are site-specific and particularly the correlation of bulk density and electrical conductivity is only rough. Therefore, further investigations by comparative measurements are necessary to verify the accuracy and utility of this methodology considering different soil types, soil compositions, and subsurface conditions.

Author Contributions: Conceptualization, M.R.; methodology, M.R. and H.S.; software, M.R. and H.S.; validation, M.R.; formal analysis, M.R.; investigation, M.R., H.S. and J.W.; resources, D.B.; data curation, M.R.; writing—original draft preparation, M.R.; writing—review and editing, M.R., H.S., J.W. and D.B.; visualization, M.R.; supervision, D.B.; project administration, D.B. and M.R.; and funding acquisition, D.B. All authors have read and agreed to the published version of the manuscript.

Funding: This research was funded in the cause of the research project 'KNW-Opt' by Federal Ministry for Economic Affairs and Climate Action (BMWK), Grant No. 03EN3020C.

Data Availability Statement: The data presented in this study are available on request from the corresponding author. The data are not publicly available due to privacy restrictions.

Acknowledgments: A big thank you goes to our research partners Stockinger and his group from the Technische Hochschule Nürnberg as well as to Stadtwerke Bad Nauheim GmbH, who provided administrative support during our measurements. In addition, thanks to the members of the shallow geothermal working group at Friedrich-Alexander Universität Erlangen-Nürnberg, especially Hannes Hagenauer and Oliver Suft, for help with the measurements and valuable discussions.

Conflicts of Interest: The authors declare no conflict of interest.

Nomenclature

Acronyms

CI	Intermediate plastic clay
CL	Low plastic clay
ERT	Electrical resistivity tomography
LSC	Large-scale geothermal collector system

Variables

θ	volumetric water content [cm^3/cm^3]
λ	thermal conductivity [W/(m·K)]
ρ_b	bulk density [g/cm^3]
ρ_w	density of water [g/cm^3]
σ_{25}	electrical conductivity at a temperature of 25 °C [S/m]
σ_T	electrical conductivity [S/m] at a temperature T
ω	gravimetric water content [g/g]
ω_L	liquid limit [g/g]
ω_P	plastic limit [g/g]
ω_S	shrinkage limit [g/g]
ER	electrical resistivity [Ω·m]
f_T	temperature correction factor [-]
I_P	plasticity index [-]
T	subsurface temperature [°C]
X_{Clay}	Correction factor for soil type group Clay [-]
X_{Silt}	Correction factor for soil type group Silt [-]

References

1. Vienken, T.; Händel, F.; Epting, J.; Dietrich, P.; Liedl, R.; Huggenberger, P. Energiewende braucht Wärmewende—Chancen und Limitierungen der intensiven thermischen Nutzung des oberflächennahen Untergrundes in urbanen Gebieten vor dem Hintergrund der aktuellen Energiedebatte in Deutschland. *Grundwasser* **2015**, *21*, 5. [CrossRef]
2. Zeh, R.; Ohlsen, B.; Philipp, D.; Bertermann, D.; Kotz, T.; Jocic, N.; Stockinger, V. Large-Scale Geothermal Collector Systems for 5th Generation District Heating and Cooling Networks. *Sustainability* **2021**, *13*, 6035. [CrossRef]
3. Boesten, S.; Ivens, W.; Dekker, S.C.; Eijdems, H. 5th generation district heating and cooling systems as a solution for renewable urban thermal energy supply. *Adv. Geosci.* **2019**, *49*, 129–136. [CrossRef]
4. Buffa, S.; Cozzini, M.; D'Antoni, M.; Baratieri, M.; Fedrizzi, R. 5th generation district heating and cooling systems: A review of existing cases in Europe. *Renew. Sustain. Energy Rev.* **2019**, *104*, 504–522. [CrossRef]
5. Di Sipio, E.; Bertermann, D. Factors Influencing the Thermal Efficiency of Horizontal Ground Heat Exchangers. *Energies* **2017**, *10*, 1897. [CrossRef]
6. Di Sipio, E.; Bertermann, D. Thermal properties variations in unconsolidated material for very shallow geothermal application (ITER project). *Int. Agrophys.* **2018**, *32*, 149–164. [CrossRef]
7. Sangi, R.; Müller, D. Dynamic modelling and simulation of a slinky-coil horizontal ground heat exchanger using Modelica. *J. Build. Eng.* **2018**, *16*, 159–168. [CrossRef]

8. Selamat, S.; Miyara, A.; Kariya, K. Analysis of Short Time Period of Operation of Horizontal Ground Heat Exchangers. *Resources* **2015**, *4*, 507–523. [CrossRef]
9. Wu, Y.; Gan, G.; Verhoef, A.; Vidale, P.L.; Gonzalez, R.G. Experimental measurement and numerical simulation of horizontal-coupled slinky ground source heat exchangers. *Appl. Therm. Eng.* **2010**, *30*, 2574–2583. [CrossRef]
10. Arning, E.; Kölling, M.; Schulz, H.D.; Panteleit, B.; Reichling, J. Einfluss oberflächennaher Wärmegewinnung auf geochemische Prozesse im Grundwasserleiter. *Grundwasser* **2006**, *11*, 27–39. [CrossRef]
11. Bonte, M.; van Breukelen, B.M.; Stuyfzand, P.J. Temperature-induced impacts on groundwater quality and arsenic mobility in anoxic aquifer sediments used for both drinking water and shallow geothermal energy production. *Water Res.* **2013**, *47*, 5088–5100. [CrossRef] [PubMed]
12. Brielmann, H.; Griebler, C.; Schmidt, S.I.; Michel, R.; Lueders, T. Effects of thermal energy discharge on shallow groundwater ecosystems. *FEMS Microbiol. Ecol.* **2009**, *68*, 273–286. [CrossRef] [PubMed]
13. Brielmann, H.; Lueders, T.; Schreglmann, K.; Ferraro, F.; Avramov, M.; Hammerl, V.; Blum, P.; Bayer, P.; Griebler, C. Oberflächennahe Geothermie und ihre potenziellen Auswirkungen auf Grundwasserökosysteme. *Grundwasser* **2011**, *16*, 77. [CrossRef]
14. Bertermann, D.; Rammler, M. Suitability of Screened Monitoring Wells for Temperature Measurements Regarding Large-Scale Geothermal Collector Systems. *Geosciences* **2022**, *12*, 162. [CrossRef]
15. Hähnlein, S.; Bayer, P.; Ferguson, G.; Blum, P. Sustainability and policy for the thermal use of shallow geothermal energy. *Energy Policy* **2013**, *59*, 914–925. [CrossRef]
16. Taylor, C.A.; Stefan, H.G. Shallow groundwater temperature response to climate change and urbanization. *J. Hydrol.* **2009**, *375*, 601–612. [CrossRef]
17. Farouki, O.T. *Thermal Properties of Soils*; Cold Regions Research and Engineering Lab: Hanover, NH, USA, 1981.
18. Bertermann, D.; Klug, H.; Morper-Busch, L.; Bialas, C. Modelling vSGPs (very shallow geothermal potentials) in selected CSAs (case study areas). *Energy* **2014**, *71*, 226–244. [CrossRef]
19. Abu-Hamdeh, N.H. Thermal Properties of Soils as affected by Density and Water Content. *Biosyst. Eng.* **2003**, *86*, 97–102. [CrossRef]
20. Abu-Hamdeh, N.H.; Reeder, R.C. Soil Thermal Conductivity Effects of Density, Moisture, Salt Concentration, and Organic Matter. *Soil Sci. Soc. Am. J.* **2000**, *64*, 1285–1290. [CrossRef]
21. Côté, J.; Konrad, J.-M. A generalized thermal conductivity model for soils and construction materials. *Can. Geotech. J.* **2011**, *42*, 443–458. [CrossRef]
22. Kersten, M. *Thermal Properties of Soils*; University of Minnesota: Mineapolis, MN, USA, 1949.
23. Lu, Y.; Lu, S.; Horton, R.; Ren, T. An Empirical Model for Estimating Soil Thermal Conductivity from Texture, Water Content, and Bulk Density. *Soil Sci. Soc. Am. J.* **2014**, *78*, 1859–1868. [CrossRef]
24. Markert, A.; Bohne, K.; Facklam, M.; Wessolek, G. Pedotransfer Functions of Soil Thermal Conductivity for the Textural Classes Sand, Silt, and Loam. *Soil Sci. Soc. Am. J.* **2017**, *81*, 1315–1327. [CrossRef]
25. Barry-Macaulay, D.; Bouazza, A.; Singh, R.M.; Wang, B.; Ranjith, P.G. Thermal conductivity of soils and rocks from the Melbourne (Australia) region. *Eng. Geol.* **2013**, *164*, 131–138. [CrossRef]
26. Low, J.E.; Loveridge, F.A.; Powrie, W.; Nicholson, D. A comparison of laboratory and in situ methods to determine soil thermal conductivity for energy foundations and other ground heat exchanger applications. *Acta Geotech.* **2015**, *10*, 209–218. [CrossRef]
27. Markert, A.; Peters, A.; Wessolek, G. Analysis of the Evaporation Method to Obtain Soil Thermal Conductivity Data in the Full Moisture Range. *Soil Sci. Soc. Am. J.* **2016**, *80*, 275–283. [CrossRef]
28. Suft, O.; Bertermann, D. One-Year Monitoring of a Ground Heat Exchanger Using the In Situ Thermal Response Test: An Experimental Approach on Climatic Effects. *Energies* **2022**, *15*, 9490. [CrossRef]
29. Zarrella, A.; Emmi, G.; Graci, S.; De Carli, M.; Cultrera, M.; Santa, G.D.; Galgaro, A.; Bertermann, D.; Müller, J.; Pockelé, L.; et al. Thermal Response Testing Results of Different Types of Borehole Heat Exchangers: An Analysis and Comparison of Interpretation Methods. *Energies* **2017**, *10*, 801. [CrossRef]
30. Dimech, A.; Cheng, L.; Chouteau, M.; Chambers, J.; Uhlemann, S.; Wilkinson, P.; Meldrum, P.; Mary, B.; Fabien-Ouellet, G.; Isabelle, A. A Review on Applications of Time-Lapse Electrical Resistivity Tomography Over the Last 30 Years: Perspectives for Mining Waste Monitoring. *Surv. Geophys.* **2022**, *43*, 1699–1759. [CrossRef]
31. Loke, M.H.; Chambers, J.E.; Rucker, D.F.; Kuras, O.; Wilkinson, P.B. Recent developments in the direct-current geoelectrical imaging method. *J. Appl. Geophys.* **2013**, *95*, 135–156. [CrossRef]
32. Loke, M.H.; Rucker, D.F.; Chambers, J.E.; Wilkinson, P.B.; Kuras, O. Electrical Resistivity Surveys and Data Interpretation. In *Encyclopedia of Solid Earth Geophysics*; Gupta, H.K., Ed.; Springer International Publishing: Cham, Switzerland, 2020; pp. 1–6.
33. Samouëlian, A.; Cousin, I.; Tabbagh, A.; Bruand, A.; Richard, G. Electrical resistivity survey in soil science: A review. *Soil Tillage Res.* **2005**, *83*, 173–193. [CrossRef]
34. Bertermann, D.; Schwarz, H. Laboratory device to analyse the impact of soil properties on electrical and thermal conductivity. *Int. Agrophys.* **2017**, *31*, 157–166. [CrossRef]
35. Logsdon, S.; Green, T.; Bonta, J.; Seyfried, M.; Evett, S. Comparison of Electrical and Thermal Conductivities for Soils from Five States. *Soil Sci.* **2010**, *175*, 573–578. [CrossRef]
36. Tokoro, T.; Ishikawa, T.; Shirai, S.; Nakamura, T. Estimation methods for thermal conductivity of sandy soil with electrical characteristics. *Soils Found.* **2016**, *56*, 927–936. [CrossRef]

37. Bai, W.; Kong, L.-W.; Guo, A. Effects of physical properties on electrical conductivity of compacted lateritic soil. *J. Rock Mech. Geotech. Eng.* **2013**, *5*, 406–411. [CrossRef]
38. Corwin, D.L.; Lesch, S.M. Apparent soil electrical conductivity measurements in agriculture. *Comput. Electron. Agric.* **2005**, *46*, 11–43. [CrossRef]
39. Ewing, R.P.; Hunt, A.G. Dependence of the Electrical Conductivity on Saturation in Real Porous Media. *Vadose Zone J.* **2006**, *5*, 731–741. [CrossRef]
40. Friedman, S.P. Soil properties influencing apparent electrical conductivity: A review. *Comput. Electron. Agric.* **2005**, *46*, 45–70. [CrossRef]
41. McCutcheon, M.C.; Farahani, H.J.; Stednick, J.D.; Buchleiter, G.W.; Green, T.R. Effect of Soil Water on Apparent Soil Electrical Conductivity and Texture Relationships in a Dryland Field. *Biosyst. Eng.* **2006**, *94*, 19–32. [CrossRef]
42. Schwarz, H.; Bertermann, D. Mediate relation between electrical and thermal conductivity of soil. *Geomech. Geophys. Geo-Energy Geo-Resour.* **2020**, *6*, 50. [CrossRef]
43. Narain Singh, D.; Kuriyan, S.J.; Chakravarthy Manthena, K. A generalised relationship between soil electrical and thermal resistivities. *Exp. Therm. Fluid Sci.* **2001**, *25*, 175–181. [CrossRef]
44. Sreedeep, S.; Reshma, A.C.; Singh, D.N. Generalized relationship for determining soil electrical resistivity from its thermal resistivity. *Exp. Therm. Fluid Sci.* **2005**, *29*, 217–226. [CrossRef]
45. Sun, Q.; Lü, C. Semiempirical correlation between thermal conductivity and electrical resistivity for silt and silty clay soils. *Geophysics* **2019**, *84*, MR99–MR105. [CrossRef]
46. Wang, J.; Zhang, X.; Du, L. A laboratory study of the correlation between the thermal conductivity and electrical resistivity of soil. *J. Appl. Geophys.* **2017**, *145*, 12–16. [CrossRef]
47. Dong, Y.; McCartney, J.S.; Lu, N. Critical Review of Thermal Conductivity Models for Unsaturated Soils. *Geotech. Geol. Eng.* **2015**, *33*, 207–221. [CrossRef]
48. Kümmerle, E. *Geologische Karte von Hessen 1:25000 5618 Friedberg*; Hessisches Landesamt für Bodenforschung: Wiesbaden, Germany, 1976.
49. Kümmerle, E. *Erläuterungen zur Geologischen Karte von Hessen 1: 25000 Blatt Nr. 5618 Friedberg*; Hessisches Landesamt für Bodenforschung: Wiesbaden, Germany, 1976; p. 247.
50. *DIN EN ISO 11272*; Soil Quality—Determination of Dry Bulk Density (ISO 11272:2017). German version EN ISO 11272:2017; Beuth Verlag GmbH: Berlin, Germany, 2017.
51. *DIN EN ISO 17892-1*; Geotechnical Investigation and Testing—Laboratory Testing of Soil—Part 1: Determination of Water Content (ISO 17892-1:2014). German Version EN ISO 17892-1:2014; Beuth Verlag GmbH: Berlin, Germany, 2015.
52. *DIN EN ISO 17892-12*; Geotechnical Investigation and Testing—Laboratory Testing of Soil—Part 12: Determination of Liquid and Plastic Limits (ISO 17892-12:2018). German version EN ISO 17892-12:2018; Beuth Verlag GmbH: Berlin, Germany, 2020.
53. Krabbe, W. Über die Schrumpfung bindiger Böden. *Mitteilungen der Hannoverschen Versuchsanstalt für Grundbau und Wasserbau* **1958**, *13*, 256–342.
54. *IEEE Std 442-1981*; IEEE Guide for Soil Thermal Resistivity Measurements. IEEE Power Engineering Society: New York, NY, USA, 1981.
55. *ASTM D5334*; Standard Test Method for Determination of Thermal Conductivity of Soil and Soft Rock by Thermal Needle Probe Procedure. ASTM International: West Conshohocken, PA, USA, 2014.
56. Sheets, K.R.; Hendrickx, J.M.H. Noninvasive Soil Water Content Measurement Using Electromagnetic Induction. *Water Resour. Res.* **1995**, *31*, 2401–2409. [CrossRef]
57. Bertermann, D.; Schwarz, H. Bulk density and water content-dependent electrical resistivity analyses of different soil classes on a laboratory scale. *Environ. Earth Sci.* **2018**, *77*, 570. [CrossRef]
58. Boivin, P.; Garnier, P.; Tessier, D. Relationship between Clay Content, Clay Type, and Shrinkage Properties of Soil Samples. *Soil Sci. Soc. Am. J.* **2004**, *68*, 1145–1153. [CrossRef]
59. Haines, W.B. The volume-changes associated with variations of water content in soil. *J. Agric. Sci.* **1923**, *13*, 296–310. [CrossRef]
60. Smith, C.W.; Hadas, A.; Dan, J.; Koyumdjisky, H. Shrinkage and Atterberg limits in relation to other properties of principal soil types in Israel. *Geoderma* **1985**, *35*, 47–65. [CrossRef]
61. Sharanya, A.G.; Mudavath, H.; Thyagaraj, T. Review of methods for predicting soil volume change induced by shrinkage. *Innov. Infrastruct. Solut.* **2021**, *6*, 116. [CrossRef]
62. Ardiansyah; Shiozawa, S.; Nishida, K. Thermal properties and shrinkage-swelling characteristic of clay soil in a tropical paddy field. *J. Jpn. Soc. Soil Phys.* **2008**, *110*, 67–77.
63. Brake, B.; Ploeg, M.; de Rooij, G. Water storage change estimation from in situ shrinkage measurements of clay soils. *Hydrol. Earth Syst. Sci.* **2013**, *17*, 1933–1949. [CrossRef]
64. Schäffer, B.; Schulin, R.; Boivin, P. Shrinkage Properties of Repacked Soil at Different States of Uniaxial Compression. *Soil Sci. Soc. Am. J.* **2013**, *77*, 1930–1943. [CrossRef]
65. Knödel, K.; Krummel, H.; Lange, G. *Handbuch zur Erkundung des Untergrundes von Deponien und Altlasten Band 3: Geophysik*; Springer: Berlin, Germany, 2005; p. 1102.

66. Zohdy, A.A.R.; Jackson, D.B. Application of deep electrical soundings for groundwater exploration in Hawaii. *Geophysics* **1969**, *34*, 584–600. [CrossRef]
67. Schäffer, R.; Sass, I. Ausbreitung und Vermischung geogener, kohlendioxidführender Thermalsole in oberflächennahem Grundwasser, Bad Nauheim. *Grundwasser* **2016**, *21*, 305–319. [CrossRef]